Fully Polarized Topological Isostatic Metamaterials in Three Dimensions

Zheng Tang,[‡] Fangyuan Ma[,‡] Feng Li[,*] Yugui Yao, and Di Zhou[†]

Key Lab of Advanced Optoelectronic Quantum Architecture and Measurement (MOE),
School of Physics, Beijing Institute of Technology, Beijing 100081, China

Topological surface states are unique to topological materials and are immune to disturbances. In isostatic lattices, mechanical topological floppy modes exhibit softness depending on the polarization relative to the terminating surface. However, in three dimensions, the polarization of topological floppy modes is disrupted by the ubiquitous mechanical Weyl lines. Here, we demonstrate, both theoretically and experimentally, the fully polarized topological mechanical phases free of Weyl lines. Floppy modes emerge exclusively on a particular surface of the three-dimensional isostatic structure, leading to the strongly asymmetric stiffness between opposing boundaries. Additionally, uniform soft strains can reversibly shift the lattice configuration to Weyl phases, switching the stiffness contrast to a trivially comparable level. Our work demonstrates the fully polarized topological mechanical phases in three dimensions, and paves the way towards engineering soft and adaptive metamaterials.

Introduction—Isostatic structures [1,2], also known as Maxwell structures [3,4], are mechanical frames that perfectly balance the degrees of freedom and constraints. These structures, ranging from molecular to architectural scales [5], are viewed as networks of nodes and links. Their significance lies in providing insights into stability and adaptability for innovative material and structure design, particularly in soft-matter systems [6–10]. Isostatic structures host zero-frequency edge modes that exhibit topological protection [11–14], because the boundary mechanical softness and rigidity remain unchanged even when disturbances or damage occur [15–17].

In one- and two-dimensional isostatic lattices, mechanical floppy modes can be "topologically fully polarized," as they emerge exclusively on a single boundary, while the opposing surface is completely devoid of floppy modes. This behavior results in a highly asymmetric contrast of boundary stiffness in a uniform structure. Fully polarized isostatic lattices establish the connection between elasticity and topological electronic band theory [18–23], laying the foundation for topological mechanics [24–35]. However, for two-dimensional isostatic lattices, this conceptual correspondence is not applicable to *out-of-plane* motions, which lack topological protection and mechanical polarization.

In three-dimensional (3D) isostatic lattices, the fully polarized topological mechanics is disrupted by the ubiquitous Weyl lines [36,37] that close the mechanical band gap

and reduce the contrast of boundary stiffness to a trivially comparable level. Recent studies have theoretically proposed 3D isostatic lattices that eliminate Weyl lines [36,38], but these designs allow floppy modes to emerge on both opposing surfaces, resulting in a stiffness contrast that is still trivially comparable. Furthermore, in the precedented experiments [37,39], the continuous mechanical junctions introduce finite bending stiffness that pushes the 3D-printed specimens beyond the isostatic point [40,41], making topological numbers undefined. Thus, the elimination of Weyl lines and full polarization of mechanical topology in 3D isostatic lattices remains challenging.

In this work, we demonstrate, both theoretically and experimentally, the fully polarized topological mechanical phase in three dimensions. Using the three-dimensional example known as the generalized pyrochlore lattice, we illustrate this topological mechanical phase and the resulting distinctive boundary elasticity. Our analytic design principle is based on the mechanical transfer matrix [42,43] that polarizes all floppy modes to concentrate on a single open boundary of the lattice, whereas the opposite surface is clear of floppy modes. Consequently, the lattice is topologically fully polarized and exhibits highly contrasting boundary mechanics.

Moreover, isostatic lattices grant uniform soft strains of the entire structure, known as Guest-Hutchinson modes [44], that reversibly shear the lattice configuration and induce transitions among topologically polarized and mechanical Weyl phases. This uniform shearing in a mechanical lattice is a nonlinear mechanism that alters the geometric configuration of all unit cells, but without inducing elastic energy. By shearing the lattice to the mechanical Weyl phase, the contrast in local stiffness is

---

reduced to a comparable level, because floppy modes arise on both parallel open surfaces of the lattice. This fully polarized mechanical phase in three dimensions, together with the freely switchable topological transition, results in advancements not possible in 2D systems [45], such as topological softness bounded to 3D dislocations, static mechanical nonreciprocity in all spatial dimensions, and topologically protected all terrain tire.

3D fully polarized topological isostatic lattices—Our prototype is a polymer 3D mechanical structure that uses pyrochlore lattice for network connectivity. Figure 1 displays two geometries of pyrochlore lattices, namely, the regular and generalized ones in (a) and (b), respectively. Figure 1(a) shows the unit cell of the regular pyrochlore lattice, with four corners at $A^{(0)} = \ell(1,1,0)/2$, $B^{(0)} = \ell(0,1,1)/2$, $C^{(0)} = \ell(1,0,1)/2$, and $D^{(0)} = \ell(0,0,0)/2$; primitive vectors $a_1^{(0)} = \ell(1,1,0)$, $a_2^{(0)} = \ell(0,1,1)$, and $a_3^{(0)} = \ell(1,0,1)$; and a length scale of $\ell = 24$ mm. In Fig. 1(b), the geometry of the generalized pyrochlore lattice deviates from the regular one, with vertex positions $X = X^{(0)} + \Delta X$ for $X = A, B, C, D$ and primitive vectors $a_i = a_i^{(0)} + \Delta a_i$ for $i = 1, 2, 3$. These geometric parameters reside in a vast 14-dimensional space (demonstrated in Supplemental Material [45]), which poses challenges for searching fully polarized topological mechanical phases. To address this, we employ the technique known as the 3D mechanical transfer matrix [45]. By decomposing the isostatic lattice into layers of lower dimensions, we

ensure that the lattice geometry associated with the transfer matrix allows for consistent growth of mechanical floppy modes from the top to the bottom layer. Remarkably, this approach substantially reduces the parameter space from 14 to just three dimensions. Figure 1 illustrates a geometric example that facilitates the consistent growth of floppy modes from top to bottom. In this configuration, we have $\Delta A = 0.053(1, 0.3, 0)$, $\Delta B = 0.053(0.55, 0, 1)$, $\Delta C = 0.053(-1, 1, -1)$, $\Delta D = 0.053(-1.8, -1, 1.2)$, and $\Delta a_{i=1,2,3} = 0$.

The unit cell of the generalized pyrochlore metamaterial consists of two polymer tetrahedra, each featuring a spherical hinge at every vertex, as depicted in Fig. 1(c). In Fig. 1(d), the A, B, C, D vertices of the white tetrahedra are connected to the A', B', C', D' tips of the green tetrahedra, enabling free rotations between neighboring bodies and eliminating bending stiffness. Within the unit cell, the site positions of the green tetrahedron [45] are give by $A' = A - a_1 + a_3$, $B' = B - a_2 + a_3$, $C' = C$, and $D' = D + a_3$. As a result, each spherical hinge provides three constraints, and each tetrahedron is connected to four hinges. A total of $(3 \times 4)/2 = 6$ constraints are imposed on a tetrahedron, balancing the six degrees of freedom of the rigid body. Consequently, the pyrochlore metamaterial is classified as an isostatic lattice due to the perfectly balanced degrees of freedom and constraints [4]. This isostatic point ensures the rigorous definition of topological mechanical indices, distinguishing them from the previously undefined topological numbers in super-isostatic structures [37,39].

Floppy modes refer to tetrahedron movements that do not deform their rigid bodies or mutual hinges, and thus do not involve elastic potential energy. Furthermore, floppy modes occur slowly, and their zero-frequency nature makes kinetic energy negligible. These properties allow us to exactly map the Newtonian statics of the metamaterial to an idealized spring-mass network, which enables the analytic study of the topological phases in static mechanical properties.

The idealized spring-mass model is established by assigning a mass particle to each site and representing each edge with a central-force Hookean spring. In both the spring-mass system and the pyrochlore metamaterial, the static mechanics are equivalent, as each set of floppy modes corresponds to undistorted spherical hinges, edges, and tetrahedral bodies. The static mechanics of the spring-mass pyrochlore model can be described by the compatibility matrix (C), which maps site displacements to spring elongations [6]. In spatially repetitive systems, the compatibility matrix can be Fourier transformed into reciprocal space [45], (C)(k), where k represents the wave vector. This compatibility matrix defines three integer-valued winding numbers,
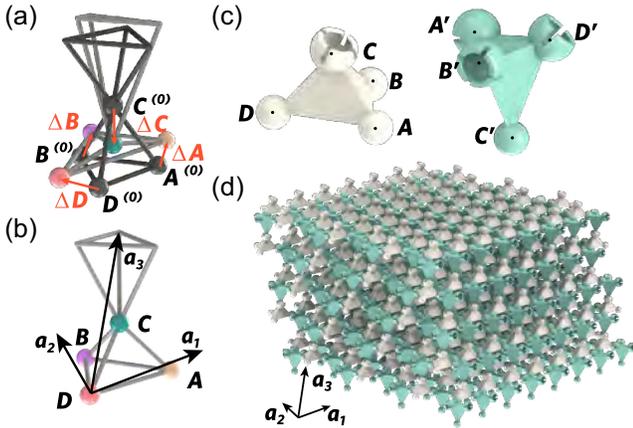

FIG. 1. Design principle of the 3D fully polarized topological mechanical metamaterial. Panels (a) and (b) describe the unit cells of the regular and generalized pyrochlore lattices, respectively, with the same primitive vectors a_1, a_2, and a_3. Each cell contains 12 bonds and 4 vertices marked by A, B, C, D. (c) The white and blue rigid bodies stand for the bottom and top tetrahedra that form the unit cell of the mechanical metamaterial. Each vertex is equipped with either a concave or convex surface, constituting the spherical hinges that allow for relative free rotations. (d) The assembly of the fully polarized topological mechanical metamaterial.

$$N_i(\mathbf{k}) = \frac{-1}{2\pi \mathrm{i}} \oint_{\mathbf{k} \to \mathbf{k} + \mathbf{b}_i} d\mathbf{k} \cdot \nabla_{\mathbf{k}} \ln \det(\mathbf{C})(\mathbf{k}), \quad i = 1, 2, 3, \quad (1)$$

that govern the topological phase of static mechanical properties, where the integration trajectory $k \to k + b_i$ follows a straight and closed loop that is parallel to the reciprocal vector b_i.

For different unit cell geometries, winding numbers can manifest qualitatively distinct behaviors. In most geometries of pyrochlore lattices, winding numbers exhibit jumps between integers as the wave vector moves across the Brillouin zone, and the critical boundaries between different integers are called mechanical Weyl lines. However, in models with gapped mechanical spectra, such as the structure exhibited in Fig. 1, winding numbers stay invariant for arbitrary wave vector, and the mechanical bands are clear of Weyl lines. These globally defined winding numbers constitute the vector [4]

$$R_{\mathrm{T}} = \sum_{i=1}^{3} N_i a_i \tag{2}$$

known as the topological polarization. This globally defined vector characterizes the topological phases of static mechanics and reflects the topological robustness of floppy modes in both the spring-mass model and the pyrochlore metamaterial. These zero-frequency mechanisms prefer to localize on the open boundary that terminates this topological polarization, while the opposite parallel boundary has fewer floppy modes.

For the lattice configuration in Fig. 1, the topological polarization is $R_{\mathrm{T}} = a_1 - a_2 - 2a_3$. As topological polarization depends on the choice of the unit cell, we introduce the local polarization vector, denoted as R_{L}. This vector characterizes how nodes and bonds are locally connected on the open surface [4,45], effectively canceling the gauge dependence of the total polarization vector, R_{T}. Together, these two polarizations govern the number density, ν, of topological floppy modes on the open surfaces of isostatic lattices. Specifically, we have $\nu = (1/2\pi)(R_{\mathrm{T}} + R_{\mathrm{L}}) \cdot G$, where G represents the reciprocal vector with its normal pointing outward from the open surface. For the pyrochlore structure shown in Fig. 1, we find the number density of the top and bottom open surfaces as $(\nu_\uparrow, \nu_\downarrow) = (0, 3)$.

The top boundary, with the floppy mode density $\nu_\uparrow = 0$, lacks any topological floppy modes entirely. In contrast, the bottom boundary hosts three floppy modes per supercell, as indicated by $\nu_\downarrow = 3$. Because of the contribution of these floppy modes to local softness, the top boundary remains as rigid as the lattice's interior, while the bottom surface becomes significantly softer than the interior. As the lattice thickness increases, the contrast ratio in edge stiffness grows exponentially due to the localization of topological floppy modes near boundaries. This exotic behavior arises uniquely from topological polarization in isostatic lattices, which we term "fully polarized topological mechanical metamaterials in 3D." In the subsequent section, we

validate this highly polarized boundary elasticity both numerically and experimentally.

It is worth emphasizing that our 3D topological lattice is fundamentally distinct from its 2D counterparts, because 2D mechanical structures are prone to deform, distort, and lose mechanical stability due to external pressure, thermal expansion, and bending [57,58]. Our work discovers the fully polarized topological mechanical phase in three dimensions. This new phase opens up avenues towards novel applications of topological mechanical metamaterials, including asymmetric wave propagation, directional polar elasticity in isostatic media, and topological fracturing protection [45].

Uniform shearing and transformable mechanical Weyl phase—Isostatic lattices are known to host nonlinear and uniform soft strains of the whole structure, namely, Guest-Hutchinson modes [1,44,59], that reversibly shear the geometry without causing any elastic energy. In the pyrochlore metamaterial, the uniform shearing represents the rotation of the top tetrahedron around the spherical hinge connecting it to the bottom tetrahedron within the unit cell. This rotational mode is uniform across all unit cells in the lattice.

The insets of Figs. 2(c) and 2(e) display two configurations of the pyrochlore unit cell that demonstrate how uniform shearing can reversibly evolve from one state to another, as visualized by the Supplemental Material, video [45]. These structures display mechanical responses that are topologically distinct from those in Fig. 2(a).
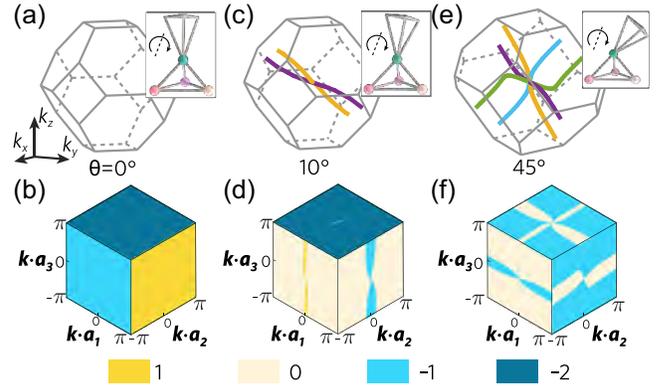

FIG. 2. Weyl lines and winding numbers in three configurations of the generalized pyrochlore lattice. (a) Brillouin zone of the generalized pyrochlore lattice without mechanical Weyl lines. The unit cell of Fig. 1(d) is described by the inset, whose black dashed line represents the rotation axis of the uniform shearing mode. (b) Winding numbers of the surface Brillouin zones of (a). (c) and (e) The Brillouin zones of the generalized pyrochlore lattice for shearing angles $\theta = 10°$ and $\theta = 45°$, containing 2 and 4 Weyl lines presented by solid color curves, respectively. (d) and (f) The winding numbers in the surface Brillouin zones corresponding to the unit cell configurations in the insets of (c) and (e), respectively.

In contrast to the globally defined winding numbers in Fig. 2(b) that originate from the fully polarized topological phase, the winding numbers in Figs. 2(d) and 2(f) can change as the wave vector moves [45]. At the critical wave vectors where the winding numbers jump, the mechanical band gap closes and form gapless lines in the 3D Brillouin zone. These are called mechanical Weyl lines [38], and are difficult to remove due to their topological robustness. The topological charge of Weyl lines [36] is determined by a nontrivial Berry phase $N_w = [(-1)/2\pi i] \times \oint_C d\mathbf{k} \cdot \nabla_\mathbf{k} \ln \det(\mathbf{C})(\mathbf{k})$, where the integration path $\mathcal{C}$ encloses the gapless lines. We highlight that the Brillouin zones depicted in Figs. 2(c) and 2(e) feature two and four Weyl lines, which correspond to a two-Weyl-line phase and a four-Weyl-line phase, respectively.

In Fig. 3(a), numerical simulations are conducted to analyze the stiffness of the top and bottom open surfaces as the uniform shearing angle increased from $\theta = 0°$ to $45°$. At $\theta = 0°$, corresponding to the configuration in Fig. 2(a), the

pyrochlore metamaterial is in the topologically fully polarized phase, exhibiting significantly higher stiffness on the top surface compared to the bottom. This strong asymmetry in surface elasticity is further corroborated by the numerical results against external poking forces shown in Fig. 3(b). Upon increasing the uniform shearing angle to $10°$, the lattice undergoes a transition into the two-Weyl-line phase, as illustrated in Fig. 2(c). This transition is characterized by a significant decrease in stiffness of the top boundary, which is quantitatively supported by the numerical analysis presented in Fig. 3(a). Further rotation of the uniform shearing angle to $45°$ induces a shift to the four-Weyl-line phase, depicted in Fig. 2(e), leading to an
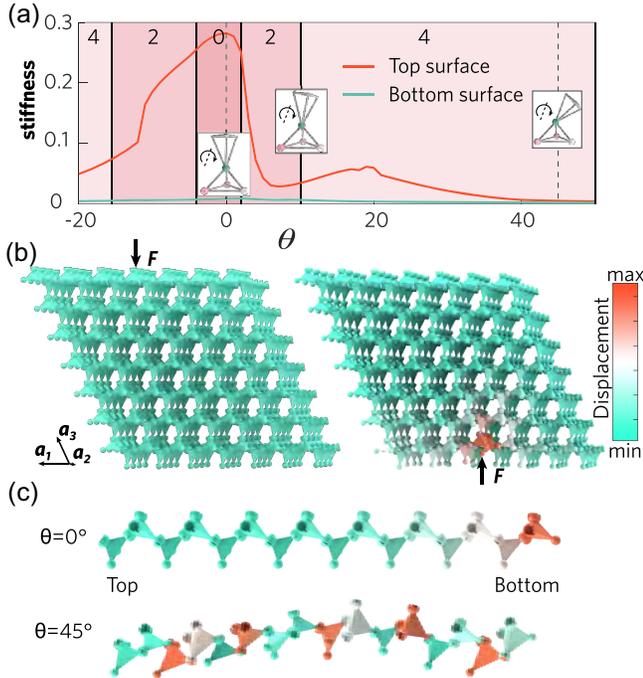

FIG. 3. Numerical simulations of the surface mechanics in the pyrochlore models under horizontal periodic boundaries and vertical open boundaries. (a) The local stiffness of top and bottom open surfaces in a model composed of $5 \times 5 \times 8$ unit cells as the uniform shearing angle θ varies. The different background colors mark topologically distinct mechanical phases, with 0, 2, and 4 denoting topologically polarized, two-Weyl-line, and four-Weyl-line phases, respectively. (b) Top and bottom surface deformations in the left and right panels, respectively, with the colors on each tetrahedron represents its center displacement. The lattice is in the topological phase (uniform shearing angle $\theta = 0°$), and is constructed from $15 \times 15 \times 8$ unit cells. (c) Spatial profiles of floppy modes in the topologically polarized and Weyl phases for the up and down panels, respectively.
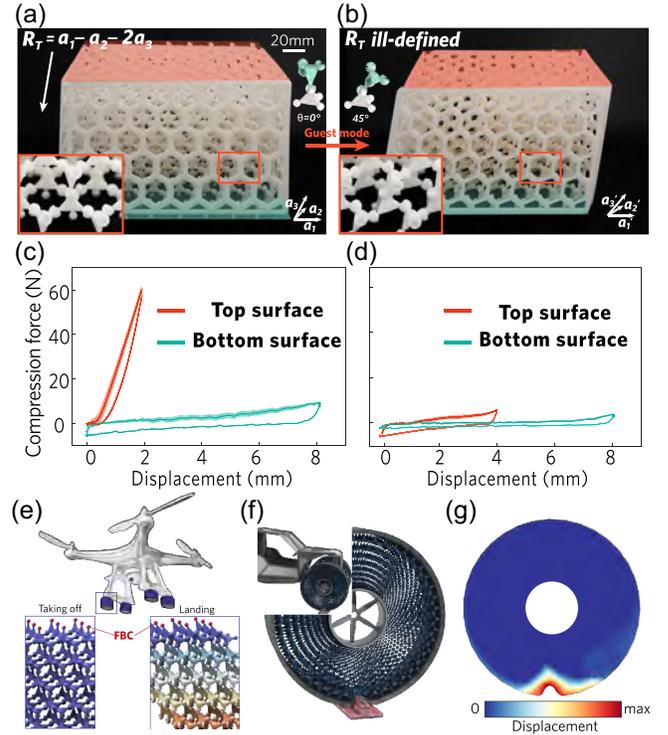

FIG. 4. Experimental measurements of the 3D-printed pyrochlore metamaterials. (a) and (b) Assembly of the 3D-printed pyrochlore lattice in topologically fully polarized and Weyl phases, respectively. The measuring open top and bottom boundaries are highlighted in red and green, whereas the four side boundaries are fixed during experimental implementations. (c) and (d) Force-displacement measurements for the topologically fully polarized and Weyl phases, respectively, where the red and green curves represent the measurements for the top and bottom boundaries. The solid lines indicate the average values, while the shaded areas represent the standard deviation across five measurements. The positive direction of displacement is defined as normal to the measuring surface when it pushes towards the interior of the lattice. (e) Topological landing gear with reconfigurable elasticity for drones. (f) Topological pyrochlore lattice incorporated into a cylindrical domain, forming a porous wheel. (g) Numerical analysis reveals the wheel's mechanical response while rolling on a rugged terrain profile.

additional reduction in stiffness of the top open surface, as evidenced by the data in Fig. 3(a). The corresponding topological mechanical phase diagram is derived in the Supplemental Material [45], exhibiting sharp and well-defined phase boundaries.

These numerical results have a direct correspondence to the boundary experiments of the 3D-printed metamaterial. In the topologically fully polarized case [Fig. 4(a)], floppy modes emerge exclusively on the bottom boundary, whereas the clearance of floppy modes on the top boundary indicates a topologically protected rigidity. This unprecedented and strongly contrasting boundary stiffness in three dimensions is experimentally demonstrated using force-displacement measurements in Fig. 4(c). We rotate the lattice's unit cell configurations by a uniform shearing angle of 45°, and the lattice structure reaches the mechanical four-Weyl-line phase in Fig. 4(b). Floppy modes arise on both the top and bottom surfaces, which is reflected by the comparable stiffness in Fig. 4(d). Here, hysteresis in the force-displacement measurements stems from the combined effects of the hinge clearance and friction. We note that the fully polarized topological and Weyl phases can be reversibly transformed by the uniform soft shearing strain.

In three dimensions, highly polarized and flexible boundary elasticity has transformative implications for various applications. Notably, our material enables switchable landing gear for drones [Fig. 4(e)]. During landing, it transitions into a soft-bottomed Weyl phase, effectively absorbing shocks. In flight, the bottom becomes a topologically rigid surface, preventing swaying. Our pyrochlore structure, applicable to continuum materials, raises the frequencies of topological floppy modes. These "soft modes" propagate asymmetrically between the top and bottom surfaces. When incorporated into a cylindrical domain, our pyrochlore structure creates porous wheels that efficiently absorb energy on rugged terrains [Figs. 4(f) and 4(g)]. Remarkably, these functionalities persist even if outer layers are removed, showcasing resilience.

Discussions—We have demonstrated, both theoretically and experimentally, the topologically fully polarized mechanical phase in three dimensions. The mechanical metamaterial remains on the isostatic point, ensuring the rigorousness of the topological mechanical index. Topological floppy modes, confined exclusively to a single boundary, result in fully polarized topological phase without Weyl lines. This mechanical achievement is analogous to the discovery of 3D topological insulators in electronic systems. Using soft uniform shearing modes, the isostatic metamaterial can be transformed from topologically polarized to Weyl phases, reducing the stiffness contrast between opposite boundaries to a trivially comparable level.

The topological polarization in three dimensions paves the way towards physics not possible for 2D lattices, such as higher-order topological floppy modes in three dimensions, topological mechanical cloaking, and static mechanical nonreciprocity in all spatial dimensions.

[1] M. Fruchart, Y. Zhou, and V. Vitelli, Nature (London) **577**, 636 (2020).

[2] H. Danawe, H. Li, K. Sun, and S. Tol, Phys. Rev. Lett. **129**, 204302 (2022).

[3] S. Papanikolaou, C. S. O'Hern, and M. D. Shattuck, Phys. Rev. Lett. **110**, 198002 (2013).

[4] C. Kane and T. Lubensky, Nat. Phys. **10**, 39 (2014).

[5] J. C. Phillips, J. Non-Cryst. Solids **34**, 153 (1979).

[6] T. Lubensky, C. Kane, X. Mao, A. Souslov, and K. Sun, Rep. Prog. Phys. **78**, 073901 (2015).

[7] H. Tong and H. Tanaka, Phys. Rev. Lett. **124**, 225501 (2020).

[8] Q.-L. Lei, F. Tang, J.-D. Hu, Y. Q. Ma, and R. Ni, Phys. Rev. Lett. **129**, 125501 (2022).

[9] J. Huang, J. Zhang, D. Xu, S. Zhang, H. Tong, and N. Xu, Current Opin. Solid State Mater. Sci. **27**, 101053 (2023).

[10] K. Bertoldi, V. Vitelli, J. Christensen, and M. Van Hecke, Nat. Rev. Mater. **2**, 17066 (2017).

[11] D. Z. Rocklin, S. Zhou, K. Sun, and X. Mao, Nat. Commun. **8**, 14201 (2017).

[12] A. Wang, Y. Zhou, and C. Q. Chen, J. Mech. Phys. Solids **173**, 105197 (2023).

[13] C. Coulais, D. Sounas, and A. Alu, Nature (London) **542**, 461 (2017).

[14] F. Ma, Z. Tang, X. Shi, Y. Wu, J. Yang, D. Zhou, Y. Yao, and F. Li, Phys. Rev. Lett. **131**, 046101 (2023).

[15] H. Xiu, I. Frankel, H. Liu, K. Qian, S. Sarkar, B. MacNider, Z. Chen, N. Boechler, and X. Mao, Proc. Natl. Acad. Sci. U.S.A. **120**, e2217928120 (2023).

[16] J. Paulose, B. G.-g. Chen, and V. Vitelli, Nat. Phys. **11**, 153 (2015).

[17] B. G.-g. Chen, N. Upadhyaya, and V. Vitelli, Proc. Natl. Acad. Sci. U.S.A. **111**, 13004 (2014).

[18] D. Xiao, M.-C. Chang, and Q. Niu, Rev. Mod. Phys. **82**, 1959 (2010).

[19] C. L. Kane and E. J. Mele, Phys. Rev. Lett. **95**, 146802 (2005).

[20] W. P. Su, J. R. Schrieffer, and A. J. Heeger, Phys. Rev. Lett. **42**, 1698 (1979).

[21] F. D. M. Haldane, Phys. Rev. Lett. **61**, 2015 (1988).

[22] X.-L. Qi and S.-C. Zhang, Rev. Mod. Phys. **83**, 1057 (2011).

[23] L. Fu, C. L. Kane, and E. J. Mele, Phys. Rev. Lett. **98**, 106803 (2007).

[24] R. Süsstrunk and S. D. Huber, Science **349**, 47 (2015).

[25] A. F. Vakakis, L. I. Manevitch, Y. V. Mikhlin, V. N. Pilipchuk, and A. A. Zevin, *Normal Modes and Localization in Nonlinear Systems* (Springer, New York, 2001).

[26] M. I. N. Rosa, R. K. Pal, J. R. F. Arruda, and M. Ruzzene, Phys. Rev. Lett. **123**, 034301 (2019).

[27] L. M. Nash, D. Kleckner, A. Read, V. Vitelli, A. M. Turner, and W. T. Irvine, Proc. Natl. Acad. Sci. U.S.A. **112,** 14495 (2015).

[28] M. Miniaci, R. K. Pal, R. Manna, and M. Ruzzene, Phys. Rev. B **100,** 024304 (2019).

[29] M. I. Rosa, M. J. Leamy, and M. Ruzzene, New J. Phys. **25,** 103053 (2023).

[30] J. R. Tempelman, K. H. Matlack, and A. F. Vakakis, Phys. Rev. B **104,** 174306 (2021).

[31] P. Wang, L. Lu, and K. Bertoldi, Phys. Rev. Lett. **115,** 104302 (2015).

[32] J. Paulose, A. S. Meeussen, and V. Vitelli, Proc. Natl. Acad. Sci. U.S.A. **112,** 7639 (2015).

[33] Q. Zhang, Y. Li, H. Sun, X. Liu, L. Zhao, X. Feng, X. Fan, and C. Qiu, Phys. Rev. Lett. **130,** 017201 (2023).

[34] J. R. Tempelman, A. F. Vakakis, and K. H. Matlack, J. Sound Vib. **568,** 118033 (2024).

[35] A. Souslov, B. C. Van Zuiden, D. Bartolo, and V. Vitelli, Nat. Phys. **13,** 1091 (2017).

[36] O. Stenull, C. L. Kane, and T. C. Lubensky, Phys. Rev. Lett. **117,** 068001 (2016).

[37] O. R. Bilal, R. Süsstrunk, C. Daraio, and S. D. Huber, Adv. Mater. **29,** 1700540 (2017).

[38] G. Baardink, A. Souslov, J. Paulose, and V. Vitelli, Proc. Natl. Acad. Sci. U.S.A. **115,** 489 (2017).

[39] A. Bergne, G. Baardink, E. G. Loukaides, and A. Souslov, Extreme Mech. Lett. **57,** 101911 (2022).

[40] K. Sun and X. Mao, Phys. Rev. Lett. **124,** 207601 (2020).

[41] O. Stenull and T. C. Lubensky, Phys. Rev. Lett. **122,** 248002 (2019).

[42] D. Zhou, L. Zhang, and X. Mao, Phys. Rev. Lett. **120,** 068003 (2018).

[43] D. Zhou, L. Zhang, and X. Mao, Phys. Rev. X **9,** 021054 (2019).

[44] S. Guest and J. Hutchinson, J. Mech. Phys. Solids **51,** 383 (2003).

[45] See Supplemental Material at http://link.aps.org/supplemental/10.1103/PhysRevLett.133.106101 for the analytic mechanical transfer matrix, the experimental setup and measurement, the topological winding numbers, and topological phase transitions. Supplemental videos show the guest mode in the pyrochlore lattice, and the force-displacement measurement. This Supplemental Material includes Refs. [46–56].

[46] Y. Long, J. Ren, and H. Chen, Proc. Natl. Acad. Sci. U.S.A. **115,** 9951 (2018).

[47] W. Cheng, K. Qian, N. Cheng, N. Boechler, X. Mao, and K. Sun, arXiv:2306.07493.

[48] J. Ma, D. Zhou, K. Sun, X. Mao, and S. Gonella, Phys. Rev. Lett. **121,** 094301 (2018).

[49] D. Zhou, D. Zeb Rocklin, M. Leamy, and Y. Yao, Nat. Commun. **13,** 3379 (2022).

[50] Y. Zhou, Y. Zhang, and C. Chen, J. Mech. Phys. Solids **153,** 104482 (2021).

[51] W. A. Benalcazar, B. A. Bernevig, and T. L. Hughes, Science **357,** 61 (2017).

[52] S. Sarkar, X. Mao, and K. Sun, Phys. Rev. B **108,** L060103 (2023).

[53] L. Zhang and X. Mao, New J. Phys. **20,** 063034 (2018).

[54] A. A. Griffith, Phil. Trans. R. Soc. A **221,** 163 (1921).

[55] T. Bückmann, M. Thiel, M. Kadic, R. Schittny, and M. Wegener, Nat. Commun. **5,** 4130 (2014).

[56] M. Lin, H. Hu, S. Zhou, and S. Xu, Nat. Rev. Mater. **7,** 850 (2022).

[57] M. Charara, J. McInerney, K. Sun, X. Mao, and S. Gonella, Proc. Natl. Acad. Sci. U.S.A. **119,** e2208051119 (2022).

[58] W. Zunker and S. Gonella, Extreme Mech. Lett. **46,** 101344 (2021).

[59] Z. Meng, M. Liu, Y. Zhang, and C. Q. Chen, J. Mech. Phys. Solids **144,** 104095 (2020).